2017-01-01

DFT Study Of Adsorption Of Trimetallic Endohedral Fullerenes On Graphene

Nakul Nitin Karle
University of Texas at El Paso, nakulkarle@gmail.com

DFT STUDY OF ADSORPTION OF TRIMETALLIC ENDOHEDRAL FULLERENES ON GRAPHENE

NAKUL NITIN KARLE

Master's Program in Computational Science

APPROVED:

Rajendra Zope, Ph.D., Chair

Tunna Baruah, Ph.D.

Mahesh Narayan, Ph.D.

Charles Ambler, Ph.D.
Dean of the Graduate School

Dedication

To Aai (Nikita Karle) and Baba (Nitin Karle)

DFT STUDY OF ADSORPTION OF TRIMETALLIC ENDOHEDRAL FULLERENES ON GRAPHENE

by

NAKUL NITIN KARLE, M.Sc., B.Sc.

THESIS

Presented to the Faculty of the Graduate School of

The University of Texas at El Paso

in Partial Fulfillment

of the Requirements

for the Degree of

MASTER OF SCIENCE

Computational Science Program

THE UNIVERSITY OF TEXAS AT EL PASO

May 2017

Acknowledgements

I would like to express my deepest gratitude to people who has helped me, encouraged me, or in some or the other way contributed to this work. These are:

Dr. Rajendra Zope, my advisor and examiner, for valuable discussions and support and for being a very nice person. He always gave me a lot of freedom to work and provided me much needed computational facilities. Thanks for giving me the opportunity to be a part of Electronic Structure Lab (ES Lab).

Dr. Tunna Baruah, for the much-needed insight to this complex world of density functional theory. Those brief discussions with you helped me improve my understanding of the subject.

Dr. Jose Ulises, for the collaboration and always taking the time to go through and suggest improvements wherever needed in my work. It was fun working with you.

One of the most important member of the ES Lab, Dr. Luis Basurto. Without you many things would have been impossible. Words will be inadequate to thank you for all the help and guidance you provided throughout my work. Thanks for keeping everyone in the lab happy and smiling all the time.

To all my friends in ES Lab, especially Dr. Yoh Yamamoto. I learned a lot from you.

To Computational Science (CPS), specially Dr. Ming-Ying Leung and Cindy Davis for their continuous support.

To all my friends at UTEP for constant motivation and their friendship. Love you all.

My roommates Dr. Paritosh Dubey and Ashesh Chattopadhyay. I was very lucky to have such nerdy roommates with whom I can always discuss my research work and ask for solutions at times of trouble.

If I forgot someone who feels that he or she should be specifically pointed out, please stop by at my place and I'll cook delicious Indian food for you…

Abstract

A density functional theory (DFT) study on the geometric and electronic structure of C_{60} and $Sc_3N@C_{80}$ along with their adsorption on pristine single layer graphene (SLG) is presented. C_{60} is found to adsorb in two nearly degenerate configurations: (i) with a pentagon facing the SLG, which is the most stable one, and (ii) with a hexagon facing the SLG in a face-to-face perfect alignment, rarely common in $\pi-\pi$ interactions, 0.06 eV higher in energy. The calculated binding energy of 0.76 eV, which includes dispersion effects, is in good agreement with previous theoretical and experimental reports. On the contrary, $Sc_3N@C_{80}$ adsorption on the SLG resulted in a higher binding energy of 1.00 eV for nearly degenerate isomers that have a pentagon and a hexagon facing the SLG. This larger binding energy is explained in terms of a higher dispersion interaction between the larger metallofullerene and the SLG, and because charge separation in $Sc_3N@C_{80}$ results in a positively charged Sc_3N inside a negatively charged C_{80}, and such an arrangement favors binding with the SLG. Furthermore, the Sc_3N moiety is found to rotate inside the supported C_{80} fullerene, which in combination with the orientation of the fullerene on the SLG leads to a series of isomers with binding energies ranging from 0.76 to 1.00 eV. $Sc_3N@C_{80}$ adsorption distance with respect to SLG is also calculated. Our results show that it could be possible to adsorb metallofulleres on SLG with an energy large enough to prevent diffusion, therefore opening the possibility to potential applications in the future technologies.

Table of Contents

List of Tables

List of Figures

Chapter 1: Introduction

This chapter gives a brief introduction to graphene, fullerenes, and endohedral fullerenes, their structural and electrical properties. A brief introduction to the density functional theory (DFT) is also provided.

1.1 Graphene

Graphene is a single layer of carbon atoms tightly packed into a 2-dimensional (2D) honeycomb lattice [Figure 1]. It is a basic building block for graphitic materials of all other dimensionalities. It is amazingly pure substance, thanks largely to its simple, orderly structure based on tight, regular, atomic bonding. Graphene can be wrapped up into a 0D Bucky balls [Figure 4], rolled into 1D nanotubes [Figure 2] or stacked into 3D graphite[1]. Carbon is a nonmetal, so it was expected that graphene will be a nonmetal as well. Astonishingly, graphene behaves much like a metal (even though the way it conducts electricity is very different from that of the metals).

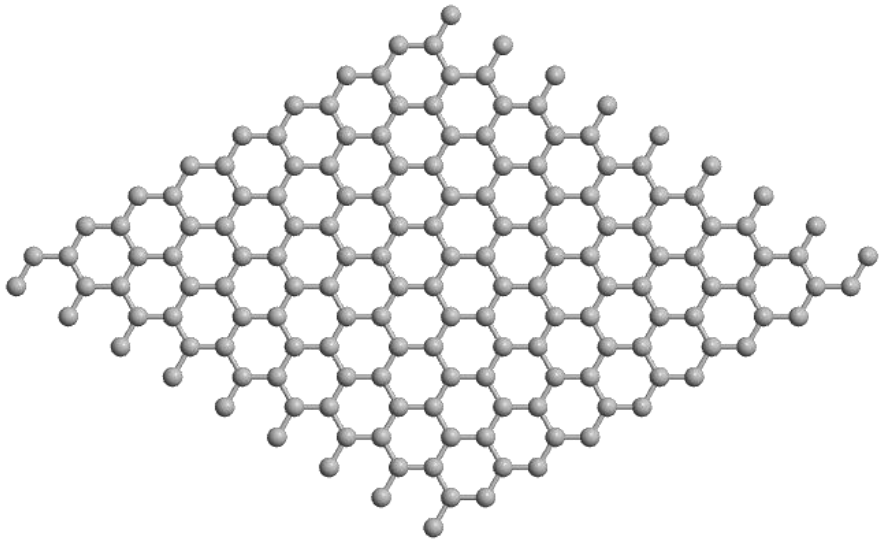

Figure 1: Pristine Single Layer Graphene (SLG)

The biggest difference between fullerenes and nanotubes with graphene is the manufacturing aspect. It is challenging to produce vast quantities of fullerenes that are pure, apart from C_{60} and C_{70}. Carbon nanotubes suffer from the problem of mixed chiralities that lead to both semiconducting and metallic electronic transport behavior. This has limited their application in electronics. On other hand, graphene manufacturing is not a big challenge with the variety of available deposition techniques. Graphene is a rising star in the field of materials science and condensed matter physics. More generally, graphene represents a conceptually new class of materials that are only one atom thick and on this basis, offers new inroads into low-dimensional physics.

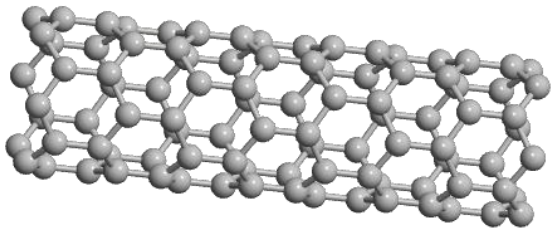

Figure 2: Nanotube

(i) Structural and electrical properties

In graphene carbon atoms are tightly bonded to each other in the honeycomb lattice structure made from hexagons and can be thought as composed of benzene rings stripped out from their hydrogen atoms. Graphene is believed to be the strongest material known, roughly 200 times stronger than steel. The structural flexibility of graphene is reflected in its electronic properties. The sp^2 hybridization between one s-orbital and two p-orbitals leads to a trigonal planar structure with a formation of σ-bond between carbon atoms which are separated by 1.42 Å. The σ-bond is responsible for the robustness of the lattice structure in all allotropes. Due to the Pauli principle,

these bands have a filled shell and hence, form a deep valence band. The unaffected p_z-orbital, which is perpendicular to the planar structure, can bind covalently with neighboring carbon atoms leading to the formation of a π bonds. Since each p-orbital has one extra electron, the π-band is half-filled[2].

Metals and insulators differ in the energy bands of their electrons. In a non-conducting material, the energy bands are either full or empty and are separated by an energy gap. In a metal, one of the bands is only partially filled. If the energy of the electron is presented as a function of their momentum, the bands become parabolas. Graphene presents an uncommon behavior, the energy bands form two circular cones, connected one with the other at their extremities [3]. They are called "Dirac Cones" [Figure 3]. However, there is no gap in between the two cones unlike insulators, but no partially filled band unlike metals. The flat hexagonal lattice of graphene offers relatively less resistance to electrons. Electrons in graphene have a longer mean free path than they have any other metal. Due to this, the graphene electrons behave in a very peculiar way. They all have the same velocity and absolutely no inertia. It is as if they have no mass, like what the theory of relativity predicts for a particle travelling with the speed of light. This property of electrons makes graphene one of the best conductor of electrons, even better than copper.

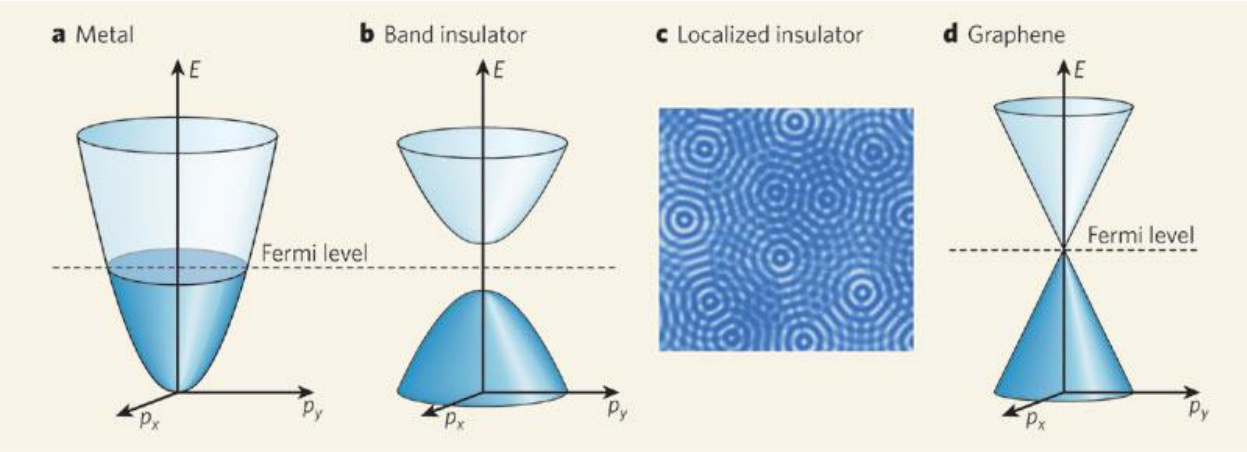

Figure 3: Metal Insulator transition

(ii) Applications

Due to its structural and electrical properties, graphene finds active applications in areas including electronics, biological engineering, filtration, lightweight/strong composite materials, photovoltaics and energy storage. Graphene has high carrier mobility, as well as low noise, allowing it to be used as the channel in a field-effect transistor. Its high electrical conductivity and high optical transparency make it a candidate for transparent conducting electrodes. Graphene would work very well in optoelectronic applications such as touchscreens, liquid crystal displays, organic photovoltaic cells and organic light emitting diodes. By very precise control over the size of the holes in the graphene sheet, graphene oxide filters could outperform other techniques of desalination by a significant margin. Due to the extremely high surface area to mass ratio of graphene, one potential application is in the conductive plates of supercapacitors. It is believed that graphene could be used to produce supercapacitors with a greater energy storage density than is currently available.

1.2 Fullerene

The Nobel Prize of the year 1996 for Chemistry was won by Harold W. Kroto, Robert F. Curl and Richard E. Smalley for their discovery in 1985 of a new allotrope of carbon, in which the atoms are arranged in closed shells. The new form was found to have the structure of truncated icosahedrons and was named Buckminsterfullerene, after the architect Buckminster Fuller who designed geodesic domes in 1960's.

Fullerenes are basically graphene sheet wrapped into 0D. They are built up of fused pentagons and hexagons. The presence of pentagons in graphene provide the curvature. Since carbon atoms are arranged spherically and hence from the physical point of view, fullerenes are 0D objects. The smallest stable and the most abundant fullerene, obtained by usual preparation methods is the I_h-symmetrical Buckminsterfullerene C_{60} [Figure 4].

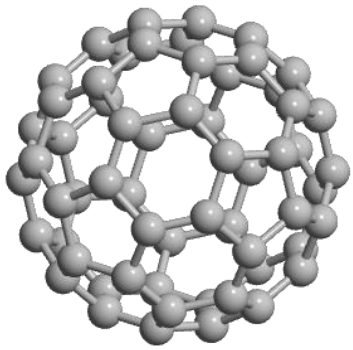

Figure 4: Fullerene (C_{60})

Buckminsterfullerene has the shape of a soccer ball. The next stable homologue is C_{70} followed by the higher fullerenes C_{74}, C_{76}, C_{78}, C_{80}, C_{82}, C_{84}, and so on. The building principle of the fullerenes is a consequence of the Euler theorem, which says that for the closure of each spherical network of n hexagons, 12 pentagons are required, except for n=1. C_{80} isomer [Figure 5] is a third icosahedral fullerene, alongside C_{20} and C_{60} and has an unstable and anti-aromatic ground state open shell structure as an empty cage.

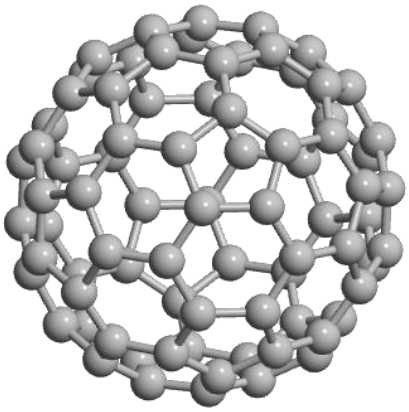

Figure 5: C_{80} - I_h

(I) Endohedral Fullerenes

The interior spaces of fullerenes can act as hosts for a variety of atoms and molecules to form endohedral fullerenes, carbon cages with one or more atoms or molecules trapped inside. Such fullerenes are called as endohedral fullerenes[4]. Endohedral fullerenes that contain clusters consisting of groups of metal atoms are known as endohedral metallofullerene. Sc_3N@Ih-C_{80} is the endohedral metallofullerene that is produced in highest quantity in the electric arc procedure for fullerene generation[5]. Empty cage fullerenes are remarkably good electron acceptors. The high electron affinity of empty fullerenes is a crucial factor for the formation of endohedral fullerenes.

$Sc_3N@I_h$-C_{80} [Figure 6] is of great interest because it's the third most abundant fullerene produced using the arc reactor. The Sc_3N unit in this is planar. In general, the metal cluster can rotate freely inside the fullerene[5]. In the preparation of M_3N-containing endohedrals, the size of the metal present determines the sizes of fullerene cages that form, with larger metal ions favoring larger cages. Thus, with scandium, a family of four Sc_3N-containing endohedrals is produced: $Sc_3N@C_{68}$, $Sc_3N@C_{78}$, and two isomers of $Sc_3N@C_{80}$ (I_h and D_{5h}). DFT calculations show that the M_3N cluster does not have preferred orientation inside I_h-C_{80} [6]. However, rotation of the metal nitride is hindered in all the cages smaller than C_{80}. Both the topology and size of the fullerene restrict the rotation of the encapsulated guest. The electronic distribution in metal nitride endohedral fullerenes may be represented by the ionic model $(M_3N)_{6+}@(C_{2n})_{6-}$. In this model, the Group 3 or lanthanide metal ions exist in their usual M_3+ state, which surround a nitride ion. Thus, six electrons are transferred from the internal cluster to the carbon cage[7].

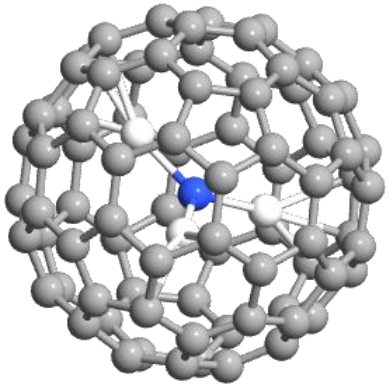

Figure 6: $Sc_3N@C_{80}$-I_h

The presence of the pentagons is compulsory to introduce curvature into the graphene surface and 12 pentagons are required to produce a closed fullerene. In C_{60} each of the thirty C–C bonds at 6:6 ring junctions is a part of a pyracylene motif as shown in [Figure 7]. The pyracylene motif places two pentagons very close to each other, while avoiding direct pentagon-pentagon contact. Thus, the pyracylene motif is not the preferential disposition to obtain maximal separation between two neighboring pentagons. As a direct consequence, fullerenes with a low number of pyracylene motifs are the most favorable hosts for metallic clusters, if a significant amount of charge is transferred. $Sc_3N@I_h$-C_{80} is the third most abundant fullerene after C_{60} and C_{70}, because it is the unique, middle-sized fullerene that lacks any pyracylene units as seen in [Figure 7]. One important thing to be noticed is that the icosahedral symmetry provides the optimal separation of 12 hexagons - 12 pentagons in case of $Sc_3N@I_h$-C_{80}, but that icosahedral symmetry itself is not a sufficient condition to encapsulate metal ions [7].

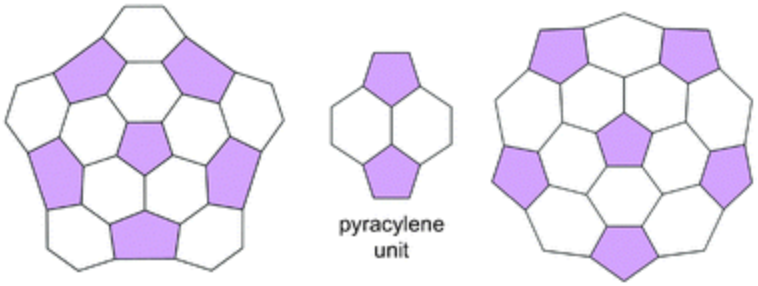

Figure 7: The basic fragments for icosahedral IPR C_{60} (left) and I_h-C_{80} (right)

(i) Structural and electrical properties

The electronic properties of endohedral fullerenes can be rationalized by the ionic model, which considers that there is a transfer of electrons from the encapsulated atoms to the carbon cage. The number of transferred electrons goes from 2e to 6e depending on the internal guest. As shown in [Figure 8], in the metallic nitride endohedral fullerenes the formal transfer of 6e from the three highest occupied orbitals of the M_3N moiety to the three low-lying unoccupied orbitals of the carbon cage occurs. Exploration of the energies of the lowest unoccupied orbitals for empty IPR fullerenes between C_{60} and C_{100} showed that the observed metal nitride M_3N endohedral metallofullerenes correspond to those IPR isomers with largest orbital gaps. In [Figure 8], we can observe that the icosahedral $I_h(7)$-C_{80} is the fullerene with largest orbital gap between these two unoccupied orbitals[6]. Black dots in [Figure 8] represent the orbital energy gap for the fullerenes that have not been observed as endohedral metallofullerenes. Fullerenes that have been observed encapsulating a metal nitride are represented in blue (IPR) and in red (non-IPR). The figure also shows schematically the formal transfer of six electrons from the highest occupied orbitals of M_3N to the lowest unoccupied (or partially occupied) orbitals of $I_h(7)$-C_{80}.

Metal nitrides (M_3N_{6+}) tend to select different cages because of the different number of transferred electrons from the internal guest to the carbon cage. Usually nitrides prefer icosahedral

isomer of C_{80}. $I_h(7)$-C_{80} are the most unstable empty isomers but become stabilized in the ionic forms when 6 electrons are added to the cage[7].

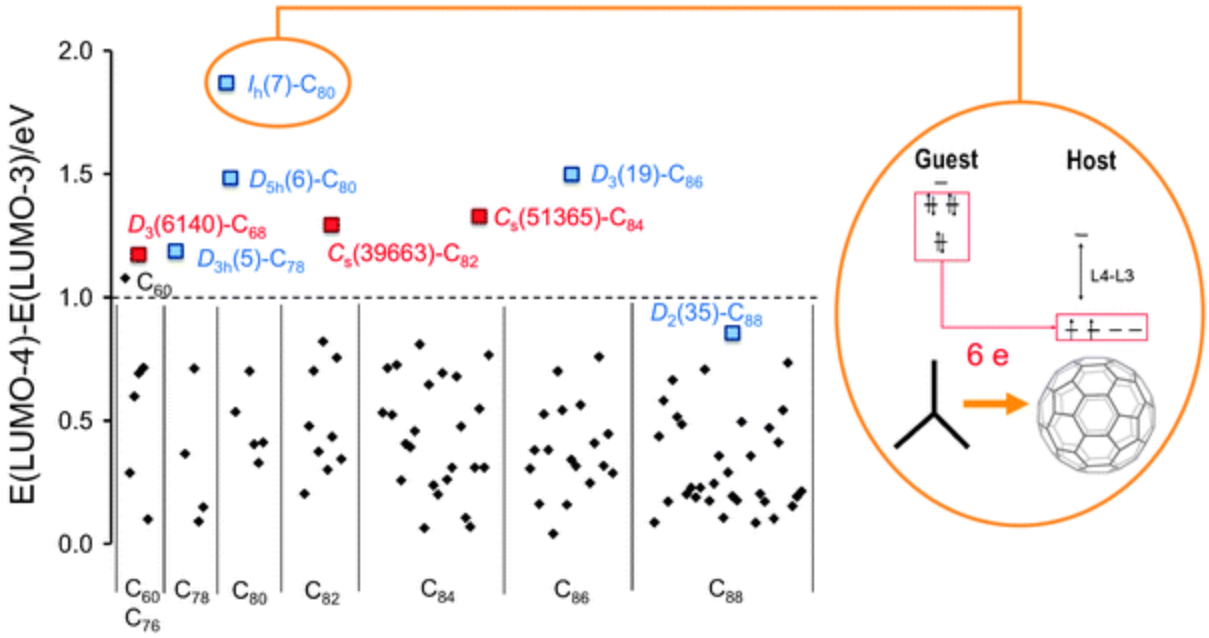

Figure 8: Gaps between the energies of the LUMO-3 and the LUMO-4 in eV for empty fullerenes between C_{60} and C_{88}

(ii) Applications

The high electron affinity and superior ability to transport charge make fullerenes the best acceptor component currently available. Hence they can be used in Organic photovoltaic cells. Due to its unique molecular structure, fullerene is the only form of carbon, which potentially can be chemically hydrogenated and de-hydrogenated reversibly. Fullerenes offer unique opportunities to harden metals and alloys without seriously compromising their ambient temperature ductility. Fullerene-based interdigitated capacitors (IDCs) recently have been developed to explore sensor

applications. This novel solid-state sensor design is based on the electron accepting properties of fullerene films and the changes that occur when planar molecules interact with the film surface. Recent experiments have documented electron transport through single molecules where fullerenes are used as molecular wires. Because of their ability to enclose atoms, fullerenes promise to be a great use as a drug carriers. Additionally, noble gases have been encapsulated in fullerenes, which have no desire to bond with the surrounding carbon atoms but can be used in applications such as magnetic resonance imaging (MRI) [8].

1.3 Density functional theory (DFT)

DFT is presently the most successful approach to compute the electronic structure of large system. It can be applied to atoms, molecules and solids. The central quantity in dft is the ground state and electron density plays a role of basic variables. DFT can predict a great variety of molecular properties like molecular structures, vibrational frequencies, atomization energies, ionization energies, electric and magnetic properties, reaction paths, etc. with reasonable accuracy.

Many body problem: The central goal in the electronic structure calculations is the solution of the time-independent, non-relativistic Schrodinger equation

$$\hat{H}\psi_i(\vec{x}_1, \vec{x}_2, \vec{x}_3, \dots\dots, \vec{x}_N, \vec{R}_1, \vec{R}_2, \vec{R}_3, \dots\dots, \vec{R}_M) = \hat{E}\,\psi_i(\vec{x}_1, \vec{x}_2, \vec{x}_3, \dots\dots, \vec{x}_N, \vec{R}_1, \vec{R}_2, \vec{R}_3, \dots\dots, \vec{R}_M)$$

(Eq. 1)

Here, $\hat{H}$ is the Hamiltonian for a system consisting of M number of nuclei and N number of electrons, $\{\vec{x}_1, \vec{x}_2, \vec{x}_3, \dots\dots, \vec{x}_N\}$ are the electronic coordinates and $\{\vec{R}_1, \vec{R}_2, \vec{R}_3, \dots\dots, \vec{R}_M\}$ are the nuclear coordinates.

$$\hat{H} = -\frac{1}{2}\sum_{i=1}^{N}\nabla_i^2 - \frac{1}{2}\sum_{A=1}^{M}\frac{1}{M_A}\nabla_i^2 - \sum_{i=1}^{N}\sum_{A=1}^{M}\frac{Z_A}{|\vec{r}_1 - \vec{R}_A|} + \sum_{i=1}^{N}\sum_{j>i}^{N}\frac{1}{|\vec{r}_i - \vec{r}_j|} + \sum_{A=1}^{M}\sum_{B>A}^{M}\frac{Z_A Z_B}{R_{AB}}$$

(Eq. 2)

Here, A and B run over the M nuclei while i and j denote the N electrons in the system. The first two terms describe the kinetic energy of the electrons and nuclei. The other three terms represent the attractive electrostatic interaction between the nuclei and the electrons and repulsive potential due to the electron-electron and nucleus-nucleus interactions.

Due to their masses the nuclei move much slower than the electrons. Hence using Born-Oppenheimer approximation, we consider the electrons as moving in the field of fixed nuclei. Therefore, the kinetic energy of the nucleus is considered zero and the potential energy is considered constant. Thus, the electronic Hamiltonian reduces to

$$\hat{H} = -\frac{1}{2}\sum_{i=1}^{N}\nabla_i^2 - \sum_{A=1}^{M}\frac{Z_A}{|\vec{r}_1 - \vec{R}_A|} + \sum_{j>i}^{N}\frac{1}{|\vec{r}_i - \vec{r}_j|} = \hat{T} + \hat{V}_{Ne} + \hat{V}_{ee}$$

(Eq. 3)

The solution of the above Schordinger equation with $< \hat{H}_{electron} >$ yields the electronic wave function $\hat{\Psi}_{electron}$ and the electronic energy $E_{electron}$. The total energy E_{total} is then the sum of $E_{electron}$ and the constant nuclear repulsion term $E_{nucleus}$.

$$\hat{H}_{electron}\hat{\Psi}_{electron} = E_{electron}\hat{\Psi}_{electron} \quad \text{(Eq. 4)}$$

$$E_{total} = E_{electron} + E_{nucleus} \quad \text{(Eq. 5)}$$

where,

$$E_{nucleus} = \sum_{A=1}^{M}\sum_{B>A}^{M}\frac{Z_A Z_B}{|\vec{R}_A - \vec{R}_B|}$$

(Eq. 6)

When a system is in the state $\widehat{\Psi}$, the expectation value of the energy is given by

$$E[\psi] = \frac{<\psi|\widehat{H}|\psi>}{<\psi|\psi>} \quad \text{(Eq. 7)}$$

$$\text{where, } <\psi|\widehat{H}|\psi> = \int \psi^* \widehat{H}\, \psi\, d\vec{x} \quad \text{(Eq. 8)}$$

The variational principle states that the energy computed from a guessed $\widehat{\Psi}$ is a upper bound to the true ground state energy E_0. Full minimization of the functional $E[\Psi]$ with respect to all allowed N-electrons wave functions will give the true ground state Ψ_0, the ground-state energy $E_0[N,V_{ext}]$, and other properties of interest. In other words, the ground state energy is a functional of the number of electrons N and the nuclear potential V_{ext}.

$$E_0 = E\,[N,V_{ext}] \quad \text{(Eq. 9)}$$

Suppose that ψ_0 (the ground state wave function) is approximated as an antisymmetrized product of N orthonormal spin orbitals $\psi_i(\vec{x})$, each a product of a spatial orbital $\phi_k(\vec{r})$ and a spin function $\sigma(s) = \alpha(s)\ or\ \beta(s)$, the Slater determinant

$$\Psi_0 \approx \psi_{HF} = \frac{1}{\sqrt{N!}} * \begin{vmatrix} \psi_1(\vec{x}_1) & \psi_2(\vec{x}_1) & \ldots\ldots\ldots & \psi_N(\vec{x}_1) \\ | & | & & | \\ \psi_1(\vec{x}_2) & \psi_2(\vec{x}_2) & \ldots\ldots\ldots & \psi_N(\vec{x}_2) \\ | & | & \ldots\ldots\ldots & | \\ \psi_1(\vec{x}_N) & \psi_2(\vec{x}_N) & \ldots\ldots\ldots & \psi_N(\vec{x}_N) \end{vmatrix}$$

The Hatree-Fock approximation is the method whereby the orthogonal orbitals ψ_i are found that minimize the energy for this determinantal form of ψ_0 :

$$E_{HF} = min_{(\psi_{HF} \to N)}\, E(\psi_{HF}) \qquad \text{(Eq. 10)}$$

The expectation value of the Hamiltonian operator with Ψ_{HF} is given by

$$E_{HF} = <\psi_{HF}|\hat{H}|\psi_{HF}> = \sum_{i=1}^{N} H_i + \frac{1}{2}\sum_{i,j=1}^{N} (J_{ij} - K_{ij}) \qquad \text{(Eq. 11)}$$

$$H_i = \int \psi_i^*(\vec{x}) \left[-\frac{1}{2}\nabla^2 - V_{external}(\vec{x}) \right] \psi_i(\vec{x})\, d\vec{x} \qquad \text{(Eq. 12)}$$

defines the contribution due to the kinetic energy and the electron-nucleus attraction and

$$J_{ij} = \iint \psi_i(\vec{x}_1)\psi_i^*(\vec{x}_1)\, \frac{1}{r_{1\cdot 2}}\, \psi_i(\vec{x}_2)\psi_j^*(\vec{x}_2)\, d\vec{x}_1\, d\vec{x}_2 \qquad \text{(Eq. 13)}$$

$$K_{ij} = \iint \psi_i(\vec{x}_1)\psi_i^*(\vec{x}_1)\, \frac{1}{r_{1\cdot 2}}\, \psi_i(\vec{x}_2)\psi_j^*(\vec{x}_2)\, d\vec{x}_1\, d\vec{x}_2 \qquad \text{(Eq. 14)}$$

The integrals are all real, and $J_{ij} \geq K_{ij} \geq 0$. The J_{ij} are called the Coulomb integrals, the K_{ij} are called the exchange integrals. Further, the minimization of the energy functional (Eq. 11) with the normalization conditions leads to the Hartree-Fock differential equations:

$$\hat{f}\psi_i = \epsilon_i \psi_i \quad , \text{i} = 1,2,3,\ldots,\text{N} \qquad \text{(Eq. 15)}$$

Where, $\hat{f}$ is an effective one-electron operator defined as

$$\hat{f} = -\frac{1}{2}\nabla_i^2 - \sum_A^M \frac{Z_A}{r_{iA}} + V_{HF}(i) \qquad \text{(Eq. 16)}$$

Density Functional Theory

The electron density is the central quantity in DFT. It is defines as follows,

$$n(\vec{r}) = N \sum_{s_1} \int d\vec{x}_2 \dots \int d\vec{x}_N \psi^*(\vec{x}_1, \vec{x}_2, \vec{x}_3, \dots\dots, \vec{x}_N)\psi(\vec{x}_1, \vec{x}_2, \vec{x}_3, \dots\dots, \vec{x}_N)$$

(Eq. 17)

$n(\vec{r})$ determines the probability of finding any of the N electrons within volume $d\vec{r}$. The integral in the equation gives the probability that an electron with arbitrary spin is found in the volume element $d\vec{r}_1$. Since the electrons are indistinguishable, N times the integral gives the probability that any electron is found there. The other electrons represented by the wave function $\psi(\vec{x}_1, \vec{x}_2, \vec{x}_3, \dots\dots, \vec{x}_N)$ have arbitrary spin and spatial coordinates.

Before representing an approach using the electron density as variable, it must be ensured that it truly contains all necessary information about the system. In detail that means it must contain information about the electron number N as well as the external potential $V_{external}$.

The total number of electrons can be obtained by the integration of the electron density over the spatial variables

$$N = \int d\vec{r}\, n(\vec{r}) \qquad \text{(Eq. 18)}$$

The first Hohenberg-Kohn theorem demonstrates that the electron density uniquely determines the Hamiltonian operator and thus all the properties of the system.

First Hohenberg-Kohn theorem: The external potential $V_{external}(\vec{r})$ is a unique functional of $n(\vec{r})$ and, up to an unimportant constant, uniquely determined by it.

It is assumed that there exist two external potentials $v(\vec{r})$ and $v'(\vec{r})$ which differ by more than just a trivial constant. Furthermore, the assumption is made, that both potentials give rise to the same

electron density $n(\vec{r})$. Furthermore, ψ and ψ' must be different, since they fulfill different Schrodinger equations. Finally, the energies E and E' associated with the particular wave function differ.

$$E_0' < E_0 + \int [v'(\vec{r}) - v(\vec{r})\,]n(\vec{r})\,d\vec{r} \qquad \text{(Eq. 19)}$$

$$E_0 < E_0' + \int [v(\vec{r}) - v'(\vec{r})\,]n(\vec{r})\,d\vec{r} \qquad \text{(Eq. 20)}$$

By summation of the above two equations we get,

$$E_0' + E_0 < E_0 + E_0' \qquad \text{(Eq. 21)}$$

The above inequality provides the proof that $v(\vec{r})$ is truly a unique functional of $n(\vec{r})$.

Second Hohenberg-Kohn theorem: The ground state energy can be derived from the electron density using variational calculus. The electron density, which provides a minimum of the ground state energy, is therefore the exact ground state density.

$$E_{v,0} = min_{n'\overrightarrow{(r)}} E_v[n'\overrightarrow{(r)}] = min_{n'\overrightarrow{(r)}}\{ \int v\overrightarrow{(r)}\, n'\, \overrightarrow{(r)}\; d\vec{r} + F\,[n'\overrightarrow{(r)}]\} \qquad \text{(Eq. 22)}$$

here, $F\,[n'\overrightarrow{(r)}]$ is a universal functional which requires no explicit knowledge of $v\overrightarrow{(r)}$.

The Kohn-Sham equations: The framework by Hohenberg and Kohn is exact, yet not very useful in actual calculations. The only possibility would be the direst use of the second Hohenberg-Kohn theorem for energy minimization, a way that is possible in general but has proven itself to be impractical. Kohn and Sham provided a practical route to obtain the ground state electron density

by simulating a fictitious non-interacting system which has the same ground state electron density. By minimizing the total energy with respect to the Kohn-Sham orbitals they arrived at a set of single-particle Schrödinger-like equations

$$\left[-\frac{1}{2}\vec{\nabla}^2 + v_{effective}(\vec{r})\right]\phi_i(\vec{r}) = \epsilon_i\phi_i(\vec{r})$$

where, j = 1,2,….,N (Eq. 23)

and

$$v_{effective}(\vec{r}) \equiv v(\overrightarrow{r}) + \int \frac{[n'(\overrightarrow{r})]}{|\vec{r}-\vec{r}'|}\, d\vec{r} + v_{exchange}(\vec{r})$$

(Eq. 24)

$$v_{exchange}(\vec{v}) \equiv \frac{\delta}{\delta n'(\vec{r})} E_{exchange}[n'(\vec{r})]|_{n'(\vec{r})=n(\vec{r})}$$

(Eq. 25)

here, $v_{effective}$ is the effective potential, $v_{exchange}$ is the exchange potential and $E_{exchange}$ is the exchange energy respectively.

The equation for the particle density is defined as

$$[n'(\overrightarrow{r})] = \sum_{j=1}^{M} |\phi_i(\vec{r})|^2$$

(Eq. 25)

The accurate ground state total energy, as one of the most important quantities, can be expressed as

$$E = \sum_j \epsilon_j + E_{exchange}[n'(\vec{r})] - \int v_{exchange}(\vec{r})\ \overrightarrow{n(r)}dv - \frac{1}{2}\int \frac{[n'\overrightarrow{(r)}]}{|\vec{r} - \vec{r}'|}\ d\vec{r}d\vec{r}'$$

(Eq. 26)

The practical application of the Kohn-Sham method requires approximation to the exchange-correlation functional. In this work we used generalized-gradient-approximation due to Perdew-Burke-Ernzerhof.

1.4 Motivation

As seen above, both graphene and fullerene have their own unique electrical properties. Hybridization of graphene and fullerene will open doors to some astonishing applications in the field of electronics, photonics, etc. Their hybridization is envisioned to create a new class of organic photovoltaic active materials with a strong electron-accepting capability characteristic of a fullerene and good charge transport properties associated with graphene. The ultimate motivation behind this DFT study was to check the possibility of endohedral metallofullerene adsorption on SLG and ensure the strength of the adsorption in terms of binding energy of the system.

Chapter 2: Computational Methods

In this chapter, all the computational methods that were used to carry out the electronic structure calculations are described in details.

2.1 NRLMOL

NRLMOL, the Naval Research Laboratory Molecular Orbital Library is a massively parallel code for electronic structure calculations on large molecules and clusters. The code is based on Kohn-Sham formulation of density functional theory and solves Kohn-Sham equations by expressing the Kohn-Sham orbitals as a linear combination of Gaussian orbitals.

(I) Methodology

All electron theoretical calculations were carried out within the density functional formalism (DFT)[9,10] and the generalized gradient approximation of Perdew, Burke and Ernzerhof (PBE96) to describe the exchange and correlation effects[11]. The electronic orbitals and eigenstates were determined by using a linear combination of Gaussian type atomic orbital molecular orbital (LCGTO) approach with the DFT formalism in NRLMOL software[12]. Electron repulsion integrals were accurately and efficiently calculated using variational mesh and the self-consistency cycle was carried out until the energies converged. All electron QZVP like quality[13] basis sets for the C, H, N and Sc atoms were used in NRLMOL. The geometry optimization with the larger basis sets is done using NRLMOL, in which symmetry unrestricted geometry optimizations employed a LBFGS method in Cartesian coordinates with a maximum force threshold of 0.001 au. All reported geometries and binding energies are based on NRLMOL calculations. The large basis sets of QZVP quality in NRLMOL have shown to have negligible basis set superposition error (BSSE) in the calculated binding energies; therefore, BSSE is not included in the results. The dispersion interaction was included using DFT-D3 parameters[14].

The binding energy of C_{60} and $Sc_3N@C_{80}$ to the SLG was calculated per equation given below

$$B.E. = E_{fullerene} + E_{graphene} - E_{complex} \quad \text{(Eq. 30)}$$

with fullerene = C_{60} and $Sc_3N@C_{80}$

Where, $E_{fullerene}$, $E_{graphene}$, and $E_{complex}$ are the total energies, including dispersion effects, for the $Sc_3N@C_{80}$, SLG, $Sc_3N@C_{80}$ with SLG species. Note that as per the above equation, a positive B.E. implies a favorable binding and that the larger the B.E., the more stable the complex formed.

Chapter 3: Results and Discussions

In this final chapter, we have all the results obtained from the above computational work and discussion about the outcome and the future work.

3.1 Pristine SLG, C_{60} and Sc_3NC_{80} Optimized Geometries and HOMO−LUMO Gaps

A pristine SLG composed of 96 C and 24 H atoms ($C_{96}H_{24}$) forming a symmetric hexagonal nanoflake, as shown in [Figure 9] is simulated. This cluster size was determined to be large enough to serve as a support for the fullerenes that were deposited at its center. In this model, hydrogen atoms were added to the dangling bonds of the carbon edge atoms to passivate them. The SLG was optimized using NRLMOL and it was found to preserve the symmetry of extended graphene with bonds in excellent agreement with the experimental C−C bond length of 1.42 Å [15].

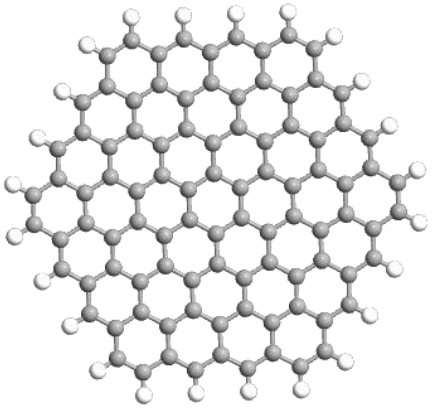

Figure 9: Graphene with C_{96} and H_{24}

The calculated gap between the highest occupied and lowest unoccupied molecular orbitals (HOMO−LUMO gap) was 1.35 eV, thus showing a semiconducting behavior in agreement with previous theoretical studies that report HOMO−LUMO gaps ranging from 0.73 to 2.89 eV depending on the cluster's size[16]. The optimized geometry in a single closed-shell configuration

for C_{60} having I_h symmetry is shown in [Figure 2]. It presents the two characteristic C−C bond lengths. The 6:6 ring bonds, between adjacent hexagons, of 1.399 Å, and the longer 6:5 bonds, between adjacent hexagons and pentagons of 1.453 Å, are in excellent agreement with the experimental values of 1.391 and 1.455 Å, respectively[17]. Furthermore, our calculated HOMO−LUMO gap for C_{60} of 1.28 eV agreed well with the previous works[18]. The optimized geometry for $Sc_3N@C_{80}$ is shown in [Figure 4]. It presents C−C bond lengths ranging from 1.435 to 1.455 Å and the endohedral moiety Sc−C and N−Sc bond lengths of 2.262 and 2.035 Å, respectively. The calculated HOMO−LUMO gap for $Sc_3N@C_{80}$ was 1.42 eV, thus exhibiting a noticeable chemical stability like C_{60}.

The special property of trimetallic nitride (M_3N) endohedral fullerenes is that there is a formal transfer of up to 6 electrons from the highest occupied orbitals of the internal moiety like Sc_3N to the three low-lying unoccupied orbitals of the carbon cage[19], which leads to stabilization of large fullerenes, which usually are highly reactive. According to experimental and theoretical studies, the endohedral Sc_3N cluster is highly mobile[20]. First evidence of its rotation was found in the experimental 13C NMR pattern, which reveals I_h symmetry, that is, the same point group as for the empty C_{80} [5]. Given that the D_{3h} symmetry of the Sc_3N cluster would lower the I_h symmetry of the $Sc_3N@C_{80}$ complex, the experimental results are only consistent with a nearly free rotation of Sc_3N, which averages out the lower symmetries. A similar rotation, and thus generation of a series of close-energy isomers, is found for the supported $Sc_3N@C_{80}$, as discussed below in section 3.3.

3.2 C_{60} Adsorption on the SLG

It was found that both C60 and Sc3N@C80 adsorbed and directly interacted with a fragment of the SLG composed of seven hexagonal carbon rings and that the second and third

carbon neighbors were less affected by the fullerenes. The optimized top and side views for the ground state and lowest energy isomer 1 and 2 of C_{60} with SLG clusters are presented in [Figure 10] and [Figure 11] respectively. The potential shows an attractive interaction that extends up to 5.5 Å. Out of the two nearly energy degenerate structures found (within a 0.065 eV energy range), the most stable one, in which a pentagon of C_{60} faces the SLG (Isomer 1), presented a tilted configuration with C(fullerene)−C(SLG) bond lengths ranging from 3.21 to 3.62 Å. These distances are within the range of distances reported using the optB86B functional in the work of Laref et al., which range from 2.81 to 3.35 Å for different absorption geometries[21] and are similar to the experimental estimation of 2.9 Å [22]. It should be noted that different cluster models and the C_{60} orientation have an important effect in the calculated geometries.

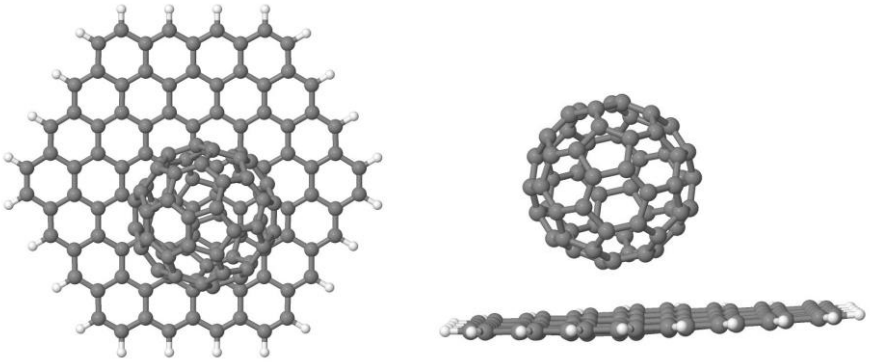

Figure 10: Isomer 1 top view and side view

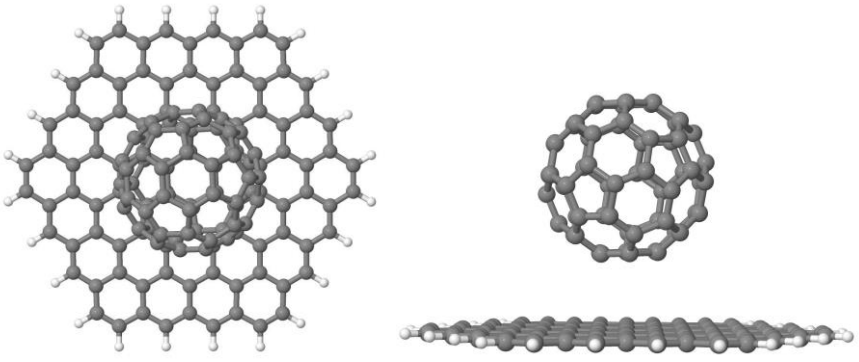

Figure 11: Isomer 2 top view and side view

We found that the SLG reacted to the C_{60} adsorption by distorting outward from planarity in the opposite side of the fullerene [Figure 10]. On the contrary, for the second energy isomer, C_{60} adsorbed a hexagon symmetrically facing the SLG in a π−π stacking interaction at 3.561 Å [Figure 12], which is within the distance range for a face-to-face perfect alignment of 3.3 to 3.8 Å, as suggested by Janiak et al. [23] based on the van der Waals radius (vdW) of the carbon atoms. Note that the reported face-to-face alignment of the rings here is extremely rare as the usual π interaction is an offset or slipped stacking; that is, the rings are parallel and displaced. The calculated B.E. is 0.76 and 0.70 eV for the most stable and lowest energy isomers, respectively. This B.E. is in good agreement with the theoretical binding energy (0.85 eV) reported by Berland et al.[24] using the vDW-DF1 van der Waals density functional and with the experimental binding energy (0.85 eV) by Ulbricht et al. [25]. Note that dispersion effects need to be considered in the theoretical modeling of the fullerene−graphene systems given that the chemical interactions of these species, dipole-induced−dipole induced, are the London dispersion intermolecular forces, as discussed below.

It should also be noted that nonpolar aromatic systems, like the system studied here, have been identified as having pi stacking (also called π−π stacking) that are attractive, noncovalent interactions which for benzene range between 0.08 and 0.12 eV. Although this is a small energy for a pair of benzene rings, this interaction accounts for the binding of larger systems with delocalized pi electrons, as shown in the experimental work of a buckycatcher by Sygula et al., in which a C_{60} binds to a convex fullerene molecule [26].

3.3 $Sc_3N@C_{80}$ Adsorption on SLG

The optimized side and top views for the ground state and four lowest energy structures of the $Sc_3N@C_{80}$-SLG systems (isomers 1 to 5) are presented in [Figure 12]. Also, shown in this Figure is the calculated interaction potential between $Sc_3N@C_{80}$ and SLG for the lowest energy

isomer as a function of the distance between them, which, as in the case of the C_{60}/SLG system, shows and attractive interaction up to 5.5 Å. The isomer reported in [Figure 12] lies within a 0.234 eV energy range above the ground-state structure and can be grouped into two sets. The first set is composed of isomer 1 (ground-state structure) and isomer 2, lies within a very close energy range of < 0.06 eV, and presents a C_{80} encapsulated Sc_3N moiety nearly perpendicular to the graphene nanoflake. The second set is composed of isomers 3 to 5 in which Sc_3N presents a parallel or slightly tilted structure with respect to the nanoflake and are between 0.15 and 0.23 eV less stable than the ground-state geometry. Note that both experimental and theoretical studies of gas-phase $Sc_3N@C_{80}$ have shown that the endohedral Sc_3N cluster is highly mobile, and we found that a similar behavior is presented in the SLG-supported cluster, although having found the previously mentioned two sets of isomers makes us think that the support tends to favor an axis of rotation of Sc_3N in orientation, in this case, perpendicular to the nanoflake plane. Furthermore, our results agree with a recent report by Osuna et al.,[27] which studies Diels−Alder additions to $Sc_3N@C_{80}$ fullerenes, and found that isomers in which two Sc atoms are pointing to the two sides of the functionalized bond (in our case toward the SLG) are the most stable ones.

All isomers in our investigation are found to present a binding of the $Sc_3N@C_{80}$ cage slightly tilted, with a 6−6 bond oriented toward the SLG and presenting similar fullerene−nanoflake bond lengths ranging from 3.02 to 3.36 Å, as shown in [Figure 12]. This distance is shorter than the one found for the C_{60}-SLG system (ranging from 3.21 to 3.60 Å) and attests for the existence of a stronger interaction of $Sc_3N@C_{80}$ with the nanoflake as compared with C_{60}.

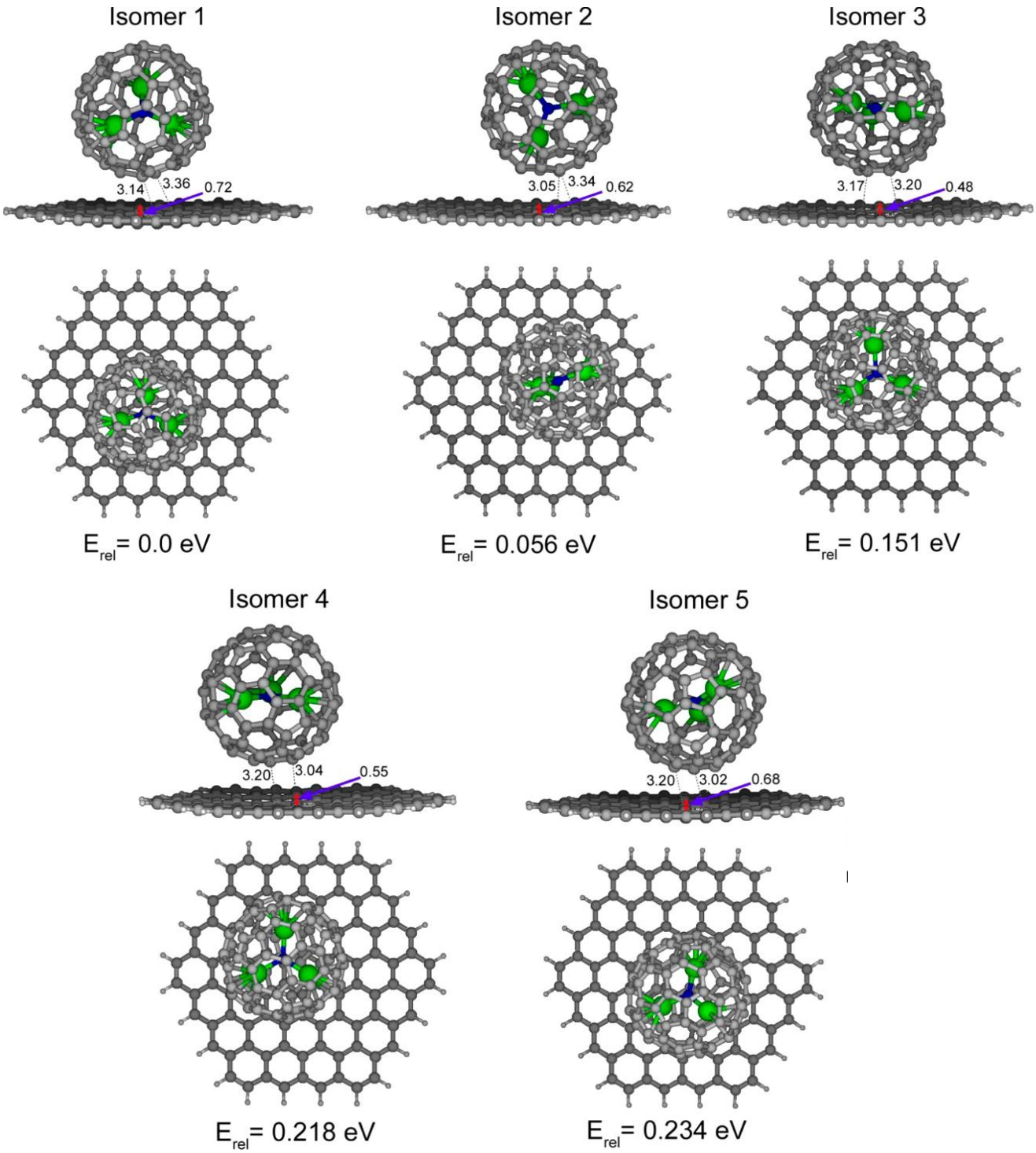

Figure 12: Side and top views for the optimized ground state and four lowest energy $Sc_3N@C_{80}$-SLG isomers.

Furthermore, an out-the-plane distortion of the nanoflake layer was found, ranging from 0.48 to 0.72 Å in the direction opposite to the side at which $Sc_3N@C_{80}$ adsorbs; this distortion gave place to a very small stretching of the C−C bond lengths of the SLG layer of < 1 pm. The B.E. of $Sc_3N@C_{80}$ to the GNF was calculated as per [Eq. 30] and gives results from 1.0 to 0.76 eV for the five $Sc_3N@C_{80}$−SLG isomers reported, thus being consistently larger that the binding energy of C60-graphene of 0.76 to 0.70 eV, as summarized in [Table 1]. As in the case of the structural analysis, this larger binding energy of $Sc_3N@C_{80}$ confirms the existence of a stronger chemical London dispersion interaction with the nanoflake, and the detail discussion about the binding mechanism can be found in section 3.4.

Table 1: Relative energy for the different isomers, dipole moment, HOMO-LUMO gap and binding energy for the SLG, C_{60}, $Sc_3N@C_{80}$, C_{60}/SLG and $Sc_3N@C_{80}$/SLG clusters

Cluster	Isomers	Relative energy (eV)	Dipole moment (debye)	HOMO-LUMO gap (eV)	Binding energy (eV)
SLG			0.92	1.35	
C60			0.00	1.28	
Sc3N@C80			0.59	1.42	
C60/SLG	1	0.00	1.15	0.69	0.76
	2	0.07	1.43	0.66	0.70
Sc3N@C80/SLG	1	0.00	1.65	1.04	1.00
	2	0.056	1.58	1.07	0.94
	3	0.151	1.17	1.01	0.85
	4	0.218	1.15	1.02	0.78
	5	0.234	1.36	1.06	0.76

3.4 Binding Mechanism and Chemical Stability

To analyze the binding mechanism of C_{60} and $Sc_3N@C_{80}$ to SLG, one-electron energy levels and molecular orbital isosurfaces for the frontier orbitals were plotted, as shown in [Figure 13]. C_{60} is a closed-shell species with sp^2 carbon atoms, forming three strong σ bonds presenting delocalized electronic π bands that surround the cage. It has a five-fold degenerated (HOMO) and a trifold degenerated (LUMO) 1.28 eV higher in energy. This large gap is a signal of chemical stability, and functionalization of the C_{60} cage has been characterized by additional reactions that transfer charge to the LUMO in bonding interaction, that is, OH addition that further enables the cage to be water-soluble by inducing local polarization[28].

On the other side, SLG's frontier orbitals presented a HOMO−LUMO gap of 1.35 eV between the two-fold degenerated HOMO and LUMO. These orbitals can be visualized by its characteristic π orbitals as a pair of symmetric lobes oriented along the z axis and centered on the nucleus. Each atom has one of these π bonds, which are then hybridized together to form what are referred to as the π-bands and π* bands, which are responsible for most of the peculiar electronic properties of graphene. Interaction between C_{60} and SLG's π bands leads to a London dispersion bonding interaction of the order of 0.76 eV, as described above. An analysis of the one electron energy levels of the C_{60}-SLG species allowed us to identify the energy levels with both C_{60} and SLG character. The 2-fold degenerated HOMO of the complex is given by SLG and the three-fold degenerated LUMO by C_{60}. Interestingly, the LUMO of C_{60} is destabilized by 0.3 eV, that is, it moves to a higher energy as compared with the free C_{60}, thus enhancing its reactivity and making it a better electron acceptor. The HOMO−LUMO gap of C_{60}-SLG is reduced to 0.69 eV because of the effect of the C_{60} adsorption.

In a similar way to C_{60}, C_{80} presents sp^2 carbon atoms and delocalized π-bands. However, in contrast with C_{60}, C_{80} is not stable by itself, and it is only after the charge transfer from the endohedral Sc_3N species to the carbon cage that it becomes a stable $Sc_3N@C_{80}$ in a closed-shell with a significant HOMO−LUMO gap of 1.42 eV.

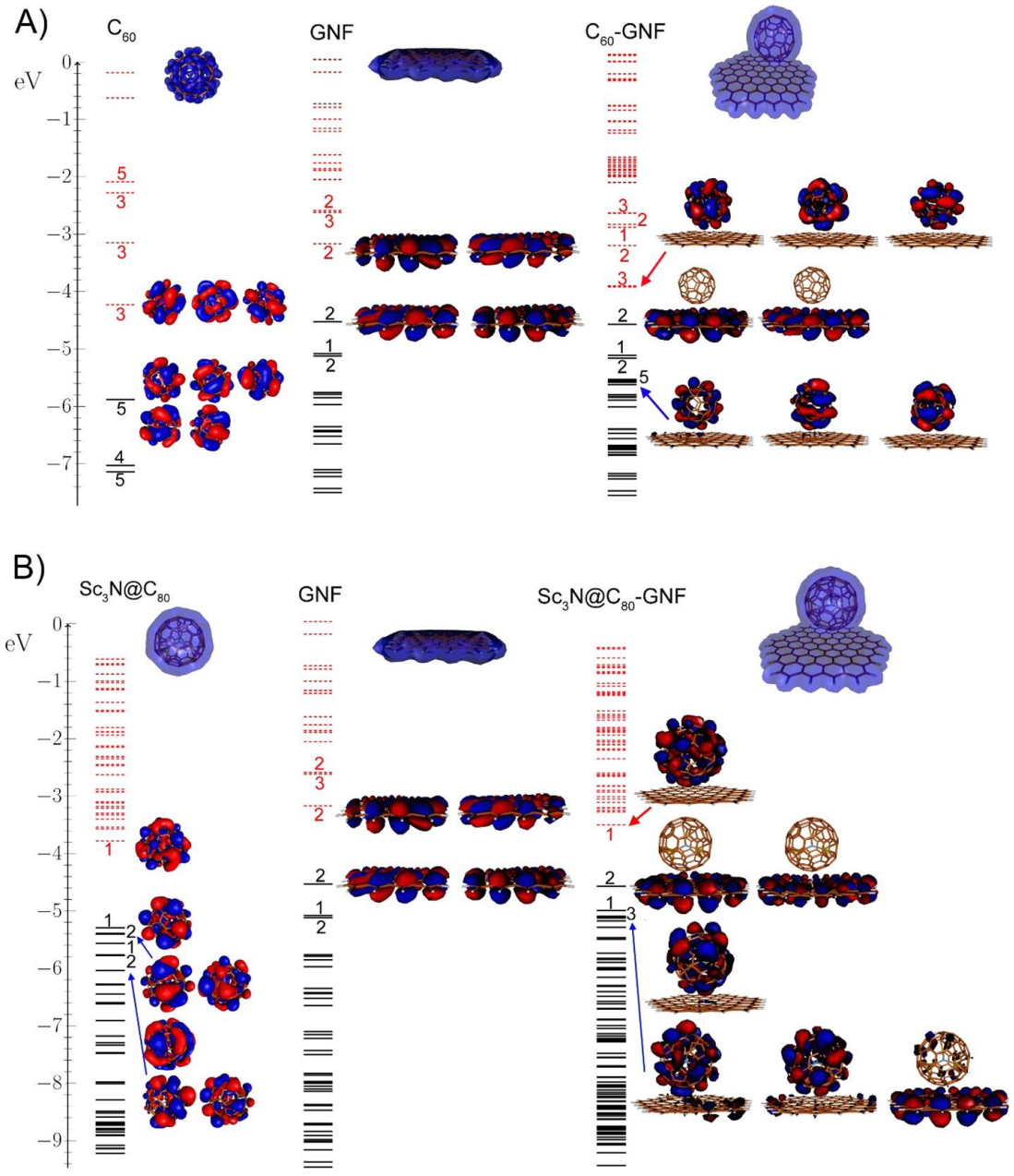

Figure 13: (A) One electron energy levels for C_{60}, SLG and C_{60}-SLG clusters, (B) $Sc_3N@C_{80}$, GNF and $Sc_3N@C_{80}$-GNF clusters. Degeneracy and isosurfaces (isoval = 0.01 au) are given for selected frontier orbitals. Solid black lines and dotted red lines represent occupied and unoccupied states.

As in the case of C_{60}-SLG, interaction between $Sc_3N@C_{80}$ and SLG's π-bands leads to a London dispersion bonding interaction ranging from 1.00 to 0.74 eV for the studied isomers [Table 1]. An analysis of the one-electron energy levels shows a HOMO and LUMO with SLG and $Sc_3N@C_{80}$ character, respectively. The LUMO of $Sc_3N@C_{80}$ is destabilized by 0.28 eV, after its absorption on to the SLG, thus enhancing its reactivity and making it a better electron acceptor. The HOMO−LUMO gap of $Sc_3N@C_{80}$-SLG is reduced from the free $Sc_3N@C_{80}$ (1.34 eV) and ranges from 1.01 to 1.07 eV for the different isomers. It is worth noting that this gap is larger than the one found for C_{60}-SLG of 0.66 eV. The formation of a chemically more stable $Sc_3N@C_{80}$ species is attributed to a stronger London dispersion intermolecular interaction between the large fullerene and graphene, as proved by the large binding energy. To investigate the effect of the fullerenes' orientation on the graphene and that of the internal degree of freedom of Sc_3N, we plot the density of states (DOS) for all of the calculated isomers in Figures 16 and 17. It can be noted that DOSs present for the two isomers of C_{60}-SLG [Figure 14] are very similar and that the found out-of-plane distortion of graphene in the ground state (0.5 Å) does not have a noticeable effect in the electronic structure, thus confirming the robustness of graphene. Similarly, the five investigated isomers for $Sc_3N@C_{80}$-SLG presented similar DOS, independently of the fullerene−nanoflake distance and position of the internal Sc_3N moiety is shown in [Figure 15].

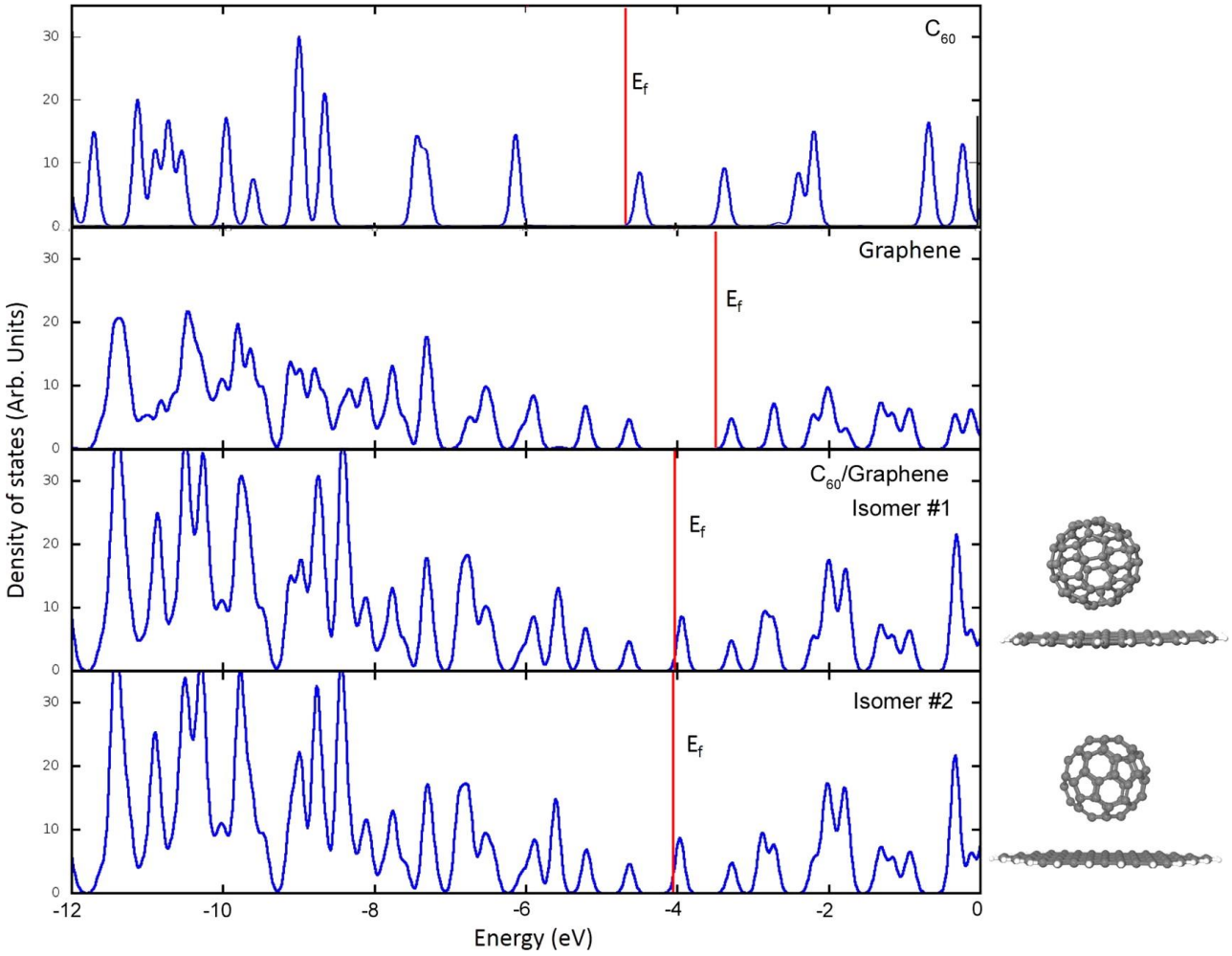

Figure 14: Density of states C_{60}, SLG and C_{60}-SLG isomer.

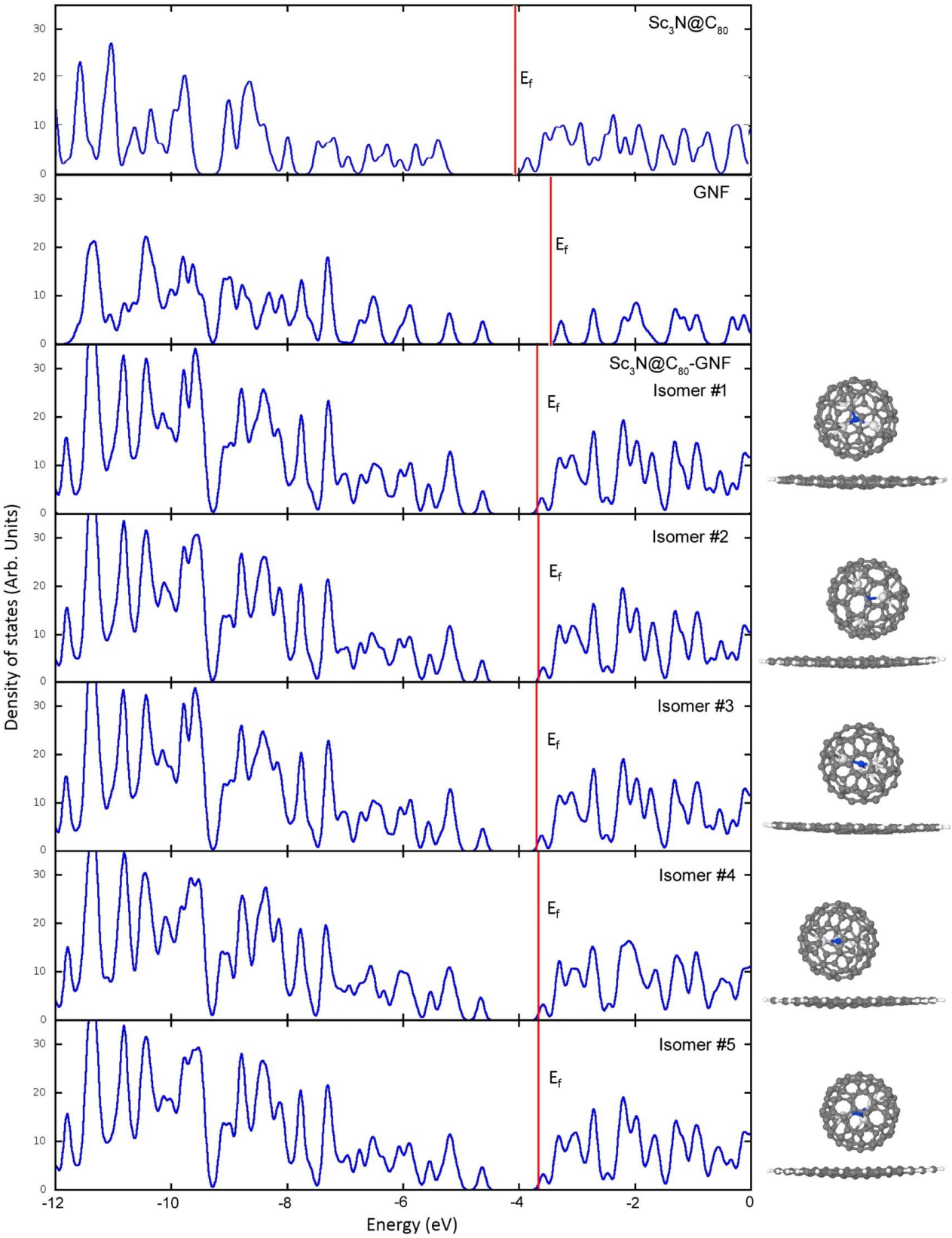

Figure 15: Density of states $Sc_3N@C_{80}$, SLG and $Sc_3N@C_{80}$-SLG isomers.

3.5 Charge Distribution and Induced Dipole Moment

One important reason to study the interaction between the $Sc_3N@C_{80}$ and SLG was the charge separation within the endohedral $Sc_3N@C_{80}$ unit. Charge transfer between Sc_3N to C_{80} stabilizes the C_{80} species, producing a positive Sc_3N core within a negative carbon cage of C_{80}. This electron-richer cage can then induce a large dispersion force with the SLG support. An analysis of the electronic charges shows that Sc_3N acquires a positive charge of 3.59 electrons, C_{80} a negative charge of −3.63 electrons, and the SLG becomes slightly positive. This charge distribution generates a dipole moment between 1.15 and 1.65 Debye for the studied isomers of $Sc_3N@C_{80}$, as shown in [Figure 16] [29].

This induced electrostatic moments may contribute to dipole−dipole induced electrostatic interactions between graphene and $Sc_3N@C_{80}$, thus being a factor that enhances the binding energy to ∼1.0 eV, compared with 0.76 eV for the C_{60}/SLG species in which only dispersion forces are present, as this system has a very small charge transfer and therefore a smaller dipole moment between 1.15 and 1.43 Debye [Table 2] [29].

Table 2: Natural Bonding Orbital (NBO) atomic charges for the different isomers of C_{60}/SLG and $Sc_3N@C_{80}$/SLG clusters

		Atomic charges				
cluster	**isomer**	**SLG**	**C_{60}**	**Sc_3N**	**C80**	**$Sc_3N@C_{80}$**
C_{60}/SLG	1	0.029	-0.029			
	2	0.018	-0.018			
$Sc_3N@C_{80}$/SLG	1	0.029		3.591	-3.620	-0.029
	2	0.025		3.584	-3.610	-0.025
	3	0.032		3.598	-3.630	-0.032
	4	0.035		3.598	-3.634	-0.035
	5	0.040		3.582	-3.690	-0.040

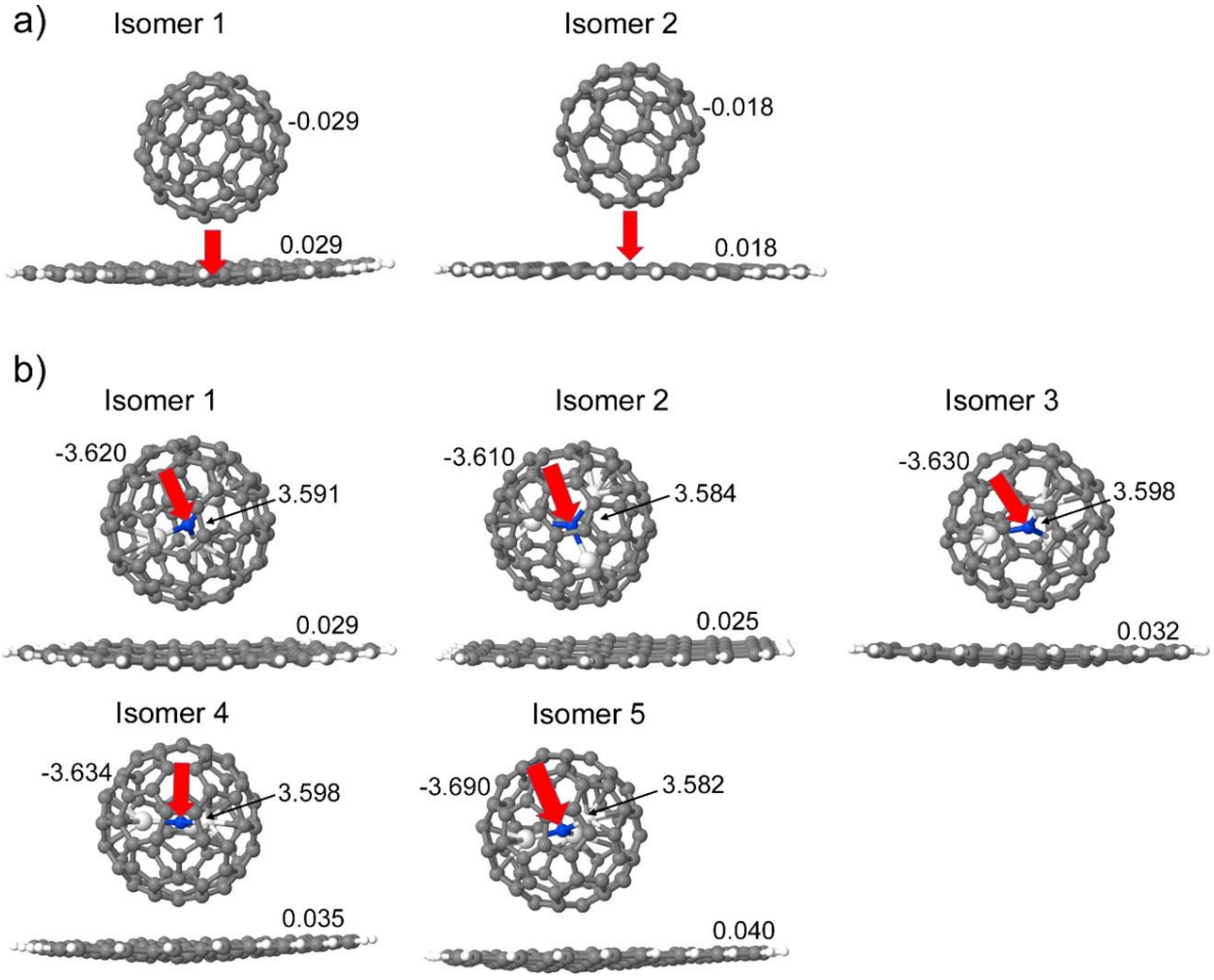

Figure 16: Electric dipole moment vector marked with a red arrow for the (a) C_{60} - SLG and (b) $Sc_3N@C_{80}$ - SLG isomers.

Chapter 4: Conclusions

An electronic and structural investigation of the interaction of a bare fullerene (C_{60}) and a larger endohedral metallofullerene ($Sc_3N@C_{80}$) with pristine single layer graphene (SLG) is presented. By explicitly including vdW corrections within the DFT framework, interactions between isolated C_{60} and $Sc_3N@C_{80}$ with pristine SLG were accurately characterized. Energetically stable geometries of both the structures are identified to be typical of physical adsorption. Our results indicate a bonding interaction resulting from London dispersion forces. C_{60} attaches with an energy of 0.76 eV and $Sc_3N@C_{80}$ with a larger energy of the order of 1.0 eV to SLG. Different isomers of $Sc_3N@C_{80}$ were explored and how the orientation of the cage and internal rotation of Sc_3N affects the binding of the system is investigated.

Two interesting facts for the C_{60}-SLG system were found. First, a low-energy isomer rarely presented a hexagonal carbon ring facing graphene in a face-to-face perfect alignment in pi-pi interactions, thus opening the possibility to use this system to investigate pi-pi interactions. Second, adsorption of C60 destabilizes its LUMO and reduces the HOMO-LUMO gap from 1.28 eV in the free C60 to only 0.69 eV on the supported cluster, thus enhancing its reactivity by making it a better electron acceptor.

The unveiled binding energies in case of $Sc_3N@C_{80}$-SLG show it could be possible to adsorb metallofullerenes on SLG without diffusion, therefore opening the possibility to potential applications especially in the field of organic photovoltaics. It will be very interesting to study the interactions of metallofullerenes with SLG containing different intrinsic point defects. Appropriate defect engineering could enable the formation of robust, thermally and mechanically stable metallofullerene-SLG lattices with interesting structural property relations.

References

(1) Geim, A. K.; Novoselov, K. S. The Rise of Graphene. *Nat. Mater.* **2007**, *6* (3), 183–191.

(2) Castro-Neto, A. H.; Peres, N. M. R.; Novoselov, K. S.; Geim, A. K. The Electronic Properties of Graphene. *Rev. Mod. Phys.* **2009**, *81* (1), 109–162.

(3) Fuhrer, M. S.; Adam, S. Condensed-Matter Physics: Carbon Conductor Corrupted. *Nature* **2009**, *458* (7234), 38–39.

(4) Chaur, M. N.; Valencia, R.; Rodríguez-Fortea, A.; Poblet, J. M.; Echegoyen, L. Trimetallic Nitride Endohedral Fullerenes: Experimental and Theoretical Evidence for the M_3N^{6+}@C2N^{6-} Model. *Angew. Chemie Int. Ed.* **2009**, *48* (8), 1425–1428.

(5) Dorn, H. C.; Stevenson, S.; Rice, G.; Glass, T.; Harich, K.; Cromer, F.; Jordan, M. R.; Craft, J.; Hadju, E.; Bible, R.; et al. Small-Bandgap Endohedral Metallofullerenes in High Yield and Purity. *Nature* **1999**, *401* (6748), 55–57.

(6) Josep M. Campanera, ‡; Carles Bo, ‡; Marilyn M. Olmstead, §; Alan L. Balch, *,§ and; Josep M. Poblet*, ‡. Bonding within the Endohedral Fullerenes Sc3N@C78 and Sc3N@C80 as Determined by Density Functional Calculations and Reexamination of the Crystal Structure of {Sc3N@C78}·Co(OEP)}·1.5(C6H6)·0.3(CHCl3). **2002**.

(7) Rodríguez-Fortea, A.; Balch, A. L.; Poblet, J. M. Endohedral Metallofullerenes: A Unique Host–guest Association. *Chem. Soc. Rev.* **2011**, *40* (7), 3551.

(8) Ulloa Eulises. Fullerenes and Their Applications in Science and Technology.

(9) Kohn, W.; Sham, L. J. Self-Consistent Equations Including Exchange and Correlation Effects. *Phys. Rev.* **1965**, *140* (4A), A1133–A1138.

(10) Hohenberg, P.; Kohn, W. Inhomogeneous Electron Gas. *Phys. Rev.* **1964**, *136* (3B), B864–B871.

(11) Perdew, J. P.; Burke, K.; Ernzerhof, M. Generalized Gradient Approximation Made Simple. *Phys. Rev. Lett.* **1996**, *77* (18), 3865–3868.

(12) Pederson, M. R.; Jackson, K. A. Variational Mesh for Quantum-Mechanical Simulations. *Phys. Rev. B* **1990**, *41* (11), 7453–7461.

(13) Porezag, D.; Pederson, M. R. Optimization of Gaussian Basis Sets for Density-Functional Calculations. *Phys. Rev. A* **1999**, *60* (4), 2840–2847.

(14) Grimme, S.; Antony, J.; Ehrlich, S.; Krieg, H. A Consistent and Accurate *Ab Initio* Parametrization of Density Functional Dispersion Correction (DFT-D) for the 94 Elements H-Pu. *J. Chem. Phys.* **2010**, *132* (15), 154104.

(15) Cooper, D. R.; D'Anjou, B.; Ghattamaneni, N.; Harack, B.; Hilke, M.; Horth, A.; Majlis, N.; Massicotte, M.; Vandsburger, L.; Whiteway, E.; et al. Experimental Review of Graphene. *ISRN Condens. Matter Phys.* **2012**, *2012*, 1–56.

(16) Silva, A. M.; Pires, M. S.; Freire, V. N.; Albuquerque, E. L.; Azevedo, D. L.; Caetano, E. W. S. Graphene Nanoflakes: Thermal Stability, Infrared Signatures, and Potential Applications in the Field of Spintronics and Optical Nanodevices. *J. Phys. Chem. C* **2010**, *114* (41), 17472–17485.

(17) David, W. I. F.; Ibberson, R. M.; Matthewman, J. C.; Prassides, K.; Dennis, T. J. S.; Hare, J. P.; Kroto, H. W.; Taylor, R.; Walton, D. R. M. Crystal Structure and Bonding of Ordered C60. *Nature* **1991**, *353* (6340), 147–149.

(18) William H. Green, J. .; Sergiu M. Gorun*, †; Fitzgerald‡, G.; Fowler, P. W.; and, A. C.; Titeca, B. C. Electronic Structures and Geometries of C60 Anions via Density Functional Calculations. **1996**.

(19) Kobayashi, K.; Sano, Y.; Nagase, S. Theoretical Study of Endohedral Metallofullerenes: Sc3?nLanN@C80 (n=0-3). *J. Comput. Chem.* **2001**, *22* (13), 1353–1358.

(20) Popov, A. A.; Zhang, L.; Dunsch, L. A Pseudoatom in a Cage: Trimetallofullerene Y_3@C_{80} Mimics Y_3N@C_{80} with Nitrogen Substituted by a Pseudoatom. *ACS Nano* **2010**, *4* (2), 795–802.

(21) Laref, S.; Asaduzzaman, A. M.; Beck, W.; Deymier, P. A.; Runge, K.; Adamowicz, L.; Muralidharan, K. Characterization of Graphene–fullerene Interactions: Insights from Density Functional Theory. *Chem. Phys. Lett.* **2013**, *582*, 115–118.

(22) Monkhorst, H. J.; Pack, J. D. Special Points for Brillouin-Zone Integrations. *Phys. Rev. B* **1976**, *13* (12), 5188–5192.

(23) Janiak, C.; Duan, C.-Y.; Hu, J.; You, X.-Z.; Mayer, P.; Scharmann, T. G.; Mayer, P.; Ramírez, J. A.; Soriano, C.; Kimura, M. A Critical Account on Π–π Stacking in Metal Complexes with Aromatic Nitrogen-Containing Ligands†. *J. Chem. Soc. Dalt. Trans.* **2000**, *38* (21), 3885–3896.

(24) Berland, K.; Hyldgaard, P. Analysis of van Der Waals Density Functional Components: Binding and Corrugation of Benzene and C 60 on Boron Nitride and Graphene. *Phys. Rev. B* **2013**, *87* (20), 205421.

(25) Ulbricht, H.; Moos, G.; Hertel, T. Interaction of C 60 with Carbon Nanotubes and Graphite. *Phys. Rev. Lett.* **2003**, *90* (9), 95501.

(26) Andrzej Sygula, *,†; Frank R. Fronczek, ‡; Renata Sygula, †; Peter W. Rabideau, † and; Olmstead§, M. M. A Double Concave Hydrocarbon Buckycatcher. **2007**.

(27) Osuna, S.; Valencia, R.; Rodríguez-Fortea, A.; Swart, M.; Solà, M.; Poblet, J. M. Full Exploration of the Diels-Alder Cycloaddition on Metallofullerenes M3N@C80 (M=Sc, Lu, Gd): The D5h versus Ih Isomer and the Influence of the Metal Cluster. *Chem. - A Eur. J.* **2012**, *18* (29), 8944–8956.

(28) Chiang, L. Y.; Swirczewski, J. W.; Hsu, C. S.; Chowdhury, S. K.; Cameron, S.; Creegan, K.; Krusic, P. J.; Wasserman, E.; Wudl, F.; Khemani, K.; et al. Multi-Hydroxy Additions onto C60 Fullerene Molecules. *J. Chem. Soc. Chem. Commun.* **1992**, *62* (24), 1791.

(29) Reveles, J. U.; Karle, N. N.; Baruah, T.; Zope, R. R. Electronic and Structural Properties of C_{60} and Sc_3N@C_{80} Supported on Graphene Nanoflakes. *J. Phys. Chem. C* **2016**, *120* (45), 26083–26092.

Vita

Nakul Nitin Karle was born in Mumbai, India. He did his B.Sc. in physics from Ramniranjan Jhunjhunwala College, Mumbai and M.Sc. in physics from the Department of Physics, University of Mumbai, India. He started his M.S. in computational science program at the University of Texas at El Paso in January 2015. In May 2017, he finished his M.S. degree.

Contact Information: nakulkarle@gmail.com

This thesis/dissertation was typed by Nakul Nitin Karle.